ADVANCES IN NUMERICAL HEAT TRANSFER

Volume 1

Edited By

W.J. Minkowycz
Professor of Mechanical Engineering
University of Illinois
Chicago, Illinois

E.M. Sparrow
Professor of Mechanical Engineering
University of Minnesota
Minneapolis, Minnesota

Taylor & Francis
Publishers since 1798

Dulikravich, G. S. and Martin, T. J., "Inverse Shape and Boundary Condition Problems and Optimization in Heat Conduction", Chapter no. 10 in ***Advances in Numerical Heat Transfer*** (editors: W. J. Minkowycz and E. M. Sparrow), Taylor and Francis, 1996, pp. 271-325.

CHAPTER
TEN

INVERSE SHAPE AND BOUNDARY CONDITION PROBLEMS AND OPTIMIZATION IN HEAT CONDUCTION

G.S. Dulikravich
T.J. Martin

1 INTRODUCTION

A heat conduction problem is fully defined (well-posed) by the following: the governing partial differential equation (elliptic for steady heat conduction and parabolic or hyperbolic for unsteady heat conduction), the thermal properties of the material (that is, the coefficients in the governing equation), the initial conditions and the boundary conditions (either of Dirichlet, Neumann or Robin type), the shape and size of the domain, and the internal heat source distribution. If any part of this information is unavailable, the problem is under-specified or ill-posed (inverse) [1]. This can happen in a number of practical situations.

For example, it is often difficult and even impossible to use sensors to measure temperatures and heat fluxes on certain boundaries such as those of combustion chambers. The placement of thermal sensors may also be impossible because of the prohibitively small size of the domain, as is the case of a computer chip or in the coolant flow passage of a turbine blade. Thus, in many cases, we are forced to solve an ill-posed boundary condition problem where the size and the shape of the domain are known, while thermal boundary conditions are unavailable on parts of the boundary and overspecified on the rest of the boundary [2–6].

A similar type of problem arises when thermal sensors cannot be used to evaluate heat sources in the domain because of the highly volatile environment as in the case of a buried toxic waste site. Thus, when the heat source distribution is partially or entirely unknown, we have to be given both temperature and heat flux data on at least a part of the boundary in order to solve this ill-posed (inverse) heat source problem [7–9].

Another class of inverse problems arises when the size and shape of some parts of the domain are unknown. In order to determine the remaining boundaries of the domain, we must know additional boundary conditions in the form of independently specified Dirichlet and Neumann boundary conditions at the same points of the known boundary. Thus, when the thermal boundary conditions are

overspecified on a part of the boundary and the remaining boundary is not known, the problem is referred to as an ill-posed (inverse) shape design problem [10-26].

The unsteady inverse heat conduction problems (UIHCP) represent a subclass of ill-posed problems which have been extensively investigated [27-31]. The UIHCP involves an estimation of the initial conditions (temperatures and heat fluxes) or an estimation of unsteady boundary conditions [27-36] (temperatures and heat fluxes) utilizing measured interior temperature histories. The major concern when attempting to solve the UIHCP computationally has been with the automatic filtering of noisy data in the discrete thermocouple measurements. The measurement data errors, as well as round-off errors, are amplified by the typical UIHCP algorithms. A review of the UIHCP literature reveals that the majority of researchers use the approach where the sum of squares of the error between the computed and measured temperatures is minimized with respect to the heat flux components. Among others, the method of regulizers [37], discrete mollification [38] against a suitable averaging kernel, and other filtering techniques [39] are usually implemented in order to smooth the extrapolated heat fluxes.

Methods for the solution of ill-posed (inverse) problems are common to a variety of engineering disciplines [40-42] and are regularly presented in the technical journals entitled *Inverse Problems* and *Inverse Problems in Engineering*. We will describe strictly our own efforts in developing fast and reliable algorithms for the solution of various inverse problems arising in heat conduction using either special non-iterative algorithms or iterative algorithms that make use of numerical optimization as a tool of achieving solutions of *de facto* inverse problems.

2 THEORETICAL FORMULATION

2.1 Steady State Heat Conduction

The governing heat conduction equation for the steady-state temperature distribution, $T(\mathbf{x})$, in a solid isotropic domain Ω bounded by the boundary Γ is given by

$$\nabla \bullet \left[k(T)\, \nabla T(\mathbf{x}) \right] + L(\mathbf{x}) = 0 \tag{1}$$

Here, $k(T)$ is the temperature-dependent coefficient of thermal conductivity, $\mathbf{x}$ is the position vector, and $L(\mathbf{x})$ is a function representing arbitrarily distributed heat sources (or sinks) per unit volume (or per unit area in case of a two-dimensional domain Ω). This quasi-linear elliptic partial differential equation can be subject to the Dirichlet (temperature) boundary conditions on the boundary Γ_1,

$$T = \overline{T} \tag{2}$$

the Neumann (heat flux Q) boundary conditions on the boundary Γ_2,

$$\frac{\partial \overline{T}}{\partial n} = \overline{Q} \tag{3}$$

and, when a boundary is exposed to a moving fluid, the Robin (convective heat transfer) boundary conditions on the boundary Γ_3

2.2 Numerical Formulation of the Heat Conduction Equation

When a partial differential equation is formulated numerically, an approximate solution, which is, in general, not the exact solution, must be used. Therefore, error, often called the residual, is introduced into problem. The weighted residual statement minimizes this error by setting the weighted sum of the residuals over the entire domain and in the boundary conditions to zero. For Poisson's equation, the weighted residual statement [43, 44] appears as

$$\int_{\Omega}\left(\nabla^2\Theta(\mathbf{y}) + f(\mathbf{y})\right) w(\mathbf{x},\mathbf{y})\, d\Omega(\mathbf{y}) + \int_{\Gamma_1}\left(\Theta(\mathbf{y}) - \overline{\Theta}(\mathbf{y})\right)\frac{\partial w(\mathbf{x},\mathbf{y})}{\partial n}\, d\Gamma(\mathbf{y}) - \int_{\Gamma_2}\left(q(\mathbf{y}) - \overline{q}(\mathbf{y})\right) w(\mathbf{x},\mathbf{y})\, d\Gamma(\mathbf{y}) = 0 \tag{10}$$

where $w(\mathbf{x},\mathbf{y})$ is the weighting function, $\mathbf{x}$ is the real space coordinate and $\mathbf{y}$ is the coordinate of integration. This statement is the starting point of most numerical formulations. The difference between them lies in how the weighting function is formulated and what approximating function is used locally.

2.3 The Boundary Element Method

The Boundary Element Method (BEM) is based upon the Green's function solution procedure. It is a very efficient numerical technique [43, 44] for solving linear boundary value problems such as those governing heat conduction, elasticity, wave propagation and electromagnetic fields. We have chosen the BEM to solve most of our inverse heat conduction problems, because it has certain distinct advantages over the more common FDM, FVM and FEM. The BEM is a non-iterative and direct solution procedure which, when used for linear boundary value problems with a small number of subdomains, is significantly faster and more robust than the other numerical solution techniques. In addition, the analytic solution to the partial differential equation, in the form of the Green's function, is part of the BEM solution. Therefore, high accuracy is expected with the BEM because introducing the Green's functions does not introduce any error into the solution.

With the BEM, the dimensionality of the problem is reduced by one order such that the unknowns are strictly confined to the boundaries, Γ, of the domain, Ω. This characteristic eliminates the need for the often difficult and time-consuming task of generating an internal boundary-conforming computational grid. In the case of inverse shape design problems where the geometry changes iteratively many times during the solution process, this benefit is invaluable. And finally, the non-iterative nature of the BEM eliminates stability, reliability and convergence problems inherent to all iterative numerical methods.

2.3.1 The boundary integral equation. The BEM begins with the weighted residual statement but is used in its weak, integral formulation. Beginning with Green's second identity procedure, we integrate the first integral in the weighted residual statement (Eq. (10)) by parts twice.

$$\int_{\Omega}\left(\nabla^2\Theta\right) w\, d\Omega = \int_{\Omega}\left(\nabla^2 w\right)\Theta\, d\Omega + \int_{\Gamma}\frac{\partial\Theta}{\partial n}\, w\, d\Gamma - \int_{\Gamma}\frac{\partial w}{\partial n}\,\Theta\, d\Gamma \tag{11}$$

We are now interested in the possibility of developing a more general method. The solution corresponding to an applied potential concentrated at a point is frequently used in boundary value problems. In the BEM, the fundamental solution, which will be represented by Θ^*, replaces the weighting function, w. The fundamental solution is a function of only the distance between the source point, **y**, and the observation point, **x**. For the two-dimensional Laplace's equation with a unit source applied at the coordinate **y**, the auxiliary Green's function solution equation is

$$\nabla^2 w + \delta(\mathbf{x}-\mathbf{y}) = \frac{d^2\Theta^*}{dr^2} + \frac{1}{r}\frac{d\Theta^*}{dr} + \delta(r) = 0 \qquad (12)$$

where the non-dimensional radial coordinate, r, is the distance from the source point to the observation node, $r = |\mathbf{x}-\mathbf{y}|/\ell$. Taking into consideration that, at the observation node, the governing equation for Θ^* equals the Dirac delta function, $\delta(r)$, the following Boundary Integral Equation (BIE) results [43, 44]

$$c(\mathbf{x})\Theta(\mathbf{x}) + \int_\Gamma q^*(\mathbf{x},\mathbf{y})\,\Theta(\mathbf{y})\,d\Gamma = \int_\Gamma \Theta^*(\mathbf{x},\mathbf{y})\,q(\mathbf{y})\,d\Gamma + \int_\Omega \Theta^*(\mathbf{x},\mathbf{y})\,f(\mathbf{y})\,d\Omega \qquad (13)$$

where

$$q^* = \frac{\partial\Theta^*}{\partial n}. \qquad (14)$$

The fundamental solution for the two-dimensional Laplace's equation is $\Theta^* = \ln(1/r)/2\pi$. When the observation node **x** is located on the boundary, Γ, the boundary integral containing the singularity must be integrated in the sense of the Cauchy principal value. Consequently, $c(\mathbf{x}) = 0$ when **x** is outside the domain, $c(\mathbf{x}) = 1.0$ when **x** is inside the domain, $c(\mathbf{x}) = \theta/2\pi$ when **x** is on the boundary, where θ is the internal angle at a corner between two neighboring boundary elements so that $c(\mathbf{x}) = 0.5$ on a smooth boundary.

2.3.2 Discretization of the BIE. The boundary, Γ, of an arbitrary multiply-connected domain, Ω, can be discretized into N_{SP} boundary elements connected between N boundary nodes. One BIE can be constructed for every boundary node under consideration. The BEM solution set can then be constructed by integrating one BIE per boundary node. In addition, the domain Ω can be discretized into N_{VC} volume cells (or area cells if the domain Ω is two-dimensional) connected between N_{TOT} nodes which include the N boundary nodes and N_{VC} volume (or area) nodes. The resulting BEM solution set contains N equations with non-dimensional temperatures, Θ, and fluxes, q, unknown on the boundary only.

$$c_i\Theta_i + \sum_{k=1}^{N_{SP}} \int_{\Gamma_k} q^*\,\Theta\,d\Gamma = \sum_{k=1}^{N_{SP}} \int_{\Gamma_k} \Theta^*\,q\,d\Gamma + \sum_{k=1}^{N_{VC}} \int_{\Omega_k} \Theta^*\,f\,d\Omega \qquad (15)$$

The variation of Θ and q can be assumed to be constant, linear, quadratic, etc. on each boundary element. The points where the values of non-dimensional temperature and flux are $\Theta_{k,j}$ and $q_{k,j}$, are called nodes. Since the nodes must also define the boundary discretization, the subscript k refers to the boundary element and the j index indicates the boundary element vertices (or boundary element endpoints).

First, we will elaborate on the discretization of two-dimensional domains, Ω, bounded by boundaries (contours), Γ. We have chosen to use a linear isoparametric representation for the boundary elements discretizing the one-dimensional boundaries (contour lines) Γ of the two-dimensional domains, Ω. The nodes on such boundary elements (contour elements) are numbered 1 and 2 and they are at the endpoints of each boundary element, respectively. The linear variation of the non-dimensional temperature along such a boundary element is then

$$\Theta(\xi) = \frac{1}{2}(1-\xi)\Theta_1 + \frac{1}{2}(1+\xi)\Theta_2 \tag{16}$$

with similar statements appearing for the flux, q, and the boundary coordinates x and y on the boundary Γ. The local dimensionless coordinate, ξ, follows the kth boundary element from $\xi = -1$ at endpoint 1 to $\xi = 1$ at endpoint 2. Then

$$d\Gamma = \left|\vec{G}\right| d\xi = \sqrt{\left(\frac{dx}{d\xi}\right)^2 + \left(\frac{dy}{d\xi}\right)^2}\, d\xi = \frac{1}{2}\sqrt{(x_2-x_1)^2 + (y_2-y_1)^2}\, d\xi \tag{17}$$

where $\left|\vec{G}\right|$ is the magnitude of the vector locally normal to the boundary, Γ.

In a similar fashion, the domain (area) cells for two-dimensional domains will be treated as isoparametric quadrilaterals where Θ_1, Θ_2, Θ_3, Θ_4 are values of the non-dimensional temperature at the four corners of a cell.

$$\Theta(\xi_1,\xi_2) = \frac{1}{4}[(1-\xi_1)(1-\xi_2)\Theta_1 + (1+\xi_1)(1-\xi_2)\Theta_2$$

$$+(1+\xi_1)(1+\xi_2)\Theta_3 + (1-\xi_1)(1+\xi_2)\Theta_4] \tag{18}$$

The origin of the ξ_1, ξ_2 local non-orthogonal coordinate system is located at the center of each two-dimensional quadrilateral cell so that the values of ξ_1 and ξ_2 are either +1 or −1 at the four corners of the quadrilateral cell. The domain integral must also be transformed using

$$d\Omega = |J|\, d\xi_1\, d\xi_2 = \det \begin{bmatrix} \frac{\partial x}{\partial \xi_1} & \frac{\partial y}{\partial \xi_1} & 0 \\ \frac{\partial x}{\partial \xi_2} & \frac{\partial y}{\partial \xi_2} & 0 \\ 0 & 0 & 1 \end{bmatrix} d\xi_1\, d\xi_2 \tag{19}$$

where $|J|$ is the Jacobian of the geometric transformation. After substitution, the BEM solution set (Eq. (15)) can be represented in the condensed matrix form as

$$[\text{diag}(\mathbf{c})]\,\{\Theta\} + [\mathbf{h}]\,\{\Theta\} = [\mathbf{g}]\,\{\mathbf{q}\} + [\mathbf{e}]\,\{\mathbf{f}\} \tag{20}$$

or in more detail as

$$\begin{bmatrix} c_1 & 0 & 0 \\ 0 & \ddots & 0 \\ 0 & 0 & c_N \end{bmatrix}\begin{Bmatrix} \Theta_1 \\ \vdots \\ \Theta_N \end{Bmatrix} + \begin{bmatrix} h_{1,1} & \cdots & h_{1,N} \\ \vdots & \ddots & \vdots \\ h_{N,1} & \cdots & h_{N,N} \end{bmatrix}\begin{Bmatrix} \Theta_1 \\ \vdots \\ \Theta_N \end{Bmatrix} = \begin{bmatrix} g_{1,1} & \cdots & g_{1,2N} \\ \vdots & \ddots & \vdots \\ g_{N,1} & \cdots & g_{N,2N} \end{bmatrix}\begin{Bmatrix} q_1 \\ \vdots \\ q_{2N} \end{Bmatrix}$$

$$+ \begin{bmatrix} e_{1,1} & \cdots & e_{1,NTOT} \\ \vdots & \ddots & \vdots \\ e_{N,1} & \cdots & e_{N,NTOT} \end{bmatrix}\begin{Bmatrix} f_1 \\ \vdots \\ f_{NTOT} \end{Bmatrix} \tag{21}$$

Since the non-dimensional temperature, Θ, is single-valued, the appropriate nodal values can be assembled together. In the case of a two-dimensional domain, Ω, each entry in the [**h**] matrix (Eq. (21)) has the following form

$$h_{i,j} = \int_{-1}^{1} \frac{1}{2}(1-\xi)\frac{-1}{2\pi\left|\mathbf{x}_i - \mathbf{y}_j(\xi)\right|}\hat{\mathbf{n}} \bullet \nabla\left|\mathbf{x}_i - \mathbf{y}_j(\xi)\right| \left|\vec{G}\right| d\xi$$

$$+ \int_{-1}^{1} \frac{1}{2}(1+\xi)\frac{-1}{2\pi\left|\mathbf{x}_i - \mathbf{y}_{j+1}(\xi)\right|}\hat{\mathbf{n}} \bullet \nabla\left|\mathbf{x}_i - \mathbf{y}_{j+1}(\xi)\right| \left|\vec{G}\right| d\xi \tag{22}$$

The unit vector, $\hat{\mathbf{n}} = \vec{G}/\left|\vec{G}\right|$, normal to the boundary Γ, arises from the chain rule

$$\frac{\partial \Theta^*}{\partial n} = \frac{\partial \Theta^*}{\partial r}\frac{\partial r}{\partial n} = \frac{\partial \Theta^*}{\partial r}\hat{\mathbf{n}} \bullet \nabla r \tag{23}$$

It should be pointed out that each entry in the [**g**] matrix is kept separate because, at a corner point on the boundary, Γ, two distinct magnitudes of flux appear at the node since $\hat{\mathbf{n}}$ is discontinuous there. In other words, at a corner, the flux on one boundary element is different from the flux on the neighboring boundary element, although they possess the same corner coordinates. Thus, a total of 2N fluxes appear in the discretized form of the BIE because for two-dimensional domains, Ω, there are the same number of boundary elements as there are boundary nodes.

The development of the BIE for three-dimensional problems is identical to the two-dimensional case except the fundamental solution is $\Theta^* = 1/4\pi r$. The boundary (surface), Γ, of the three-dimensional domain (volume), Ω, can be discretized into either triangular or quadrilateral boundary elements (surface panels). The domain (volume) can be discretized into tetrahedral or hexahedral cells. In three-dimensional problems, we have chosen to use isoparametric quadrilateral surface panels and hexahedral volume cells because of their structured nature.

2.3.3 Singular integrals. The integrals $h_{i,j}$ and $g_{i,k}$ can be calculated using the simple Gauss quadrature rule for all boundary elements except the two integrals where the observation node is at one of the vertices of the boundary element being integrated (a singularity). For two-dimensional problems with linear isoparametric elements, these integrals can be easily computed analytically. The $h_{i,i}$ term is identically zero because the vectors $\hat{\mathbf{n}}$ and $\hat{\mathbf{r}}$ are orthogonal over the boundary element when the observation node is on the boundary element. The [**g**] integrals (Eq. (21)) can be calculated analytically when the observation node is at vertex 1 or at vertex 2 as follows

$$g_{1,k,1} = \frac{s}{2}\left(\frac{3}{2} - \ln(s)\right) \quad \text{and} \quad g_{1,k,2} = \frac{s}{2}\left(\frac{1}{2} - \ln(s)\right) \tag{24}$$

where the length of the boundary element is $s = \sqrt{(x_2 - x_1)^2 + (y_2 - y_1)^2}$.

A similar situation arises in three-dimensional problems when the volume cell contains a singularity at one of its vertices. Since this integral cannot be computed analytically, an integral transformation rule is recommended [45]. A cubic variable transformation is valid for any location of the singular point. Each variable of integration, ξ_ℓ, is thus represented in terms of a new variable, γ, as

$$\xi_\ell = a\gamma^3 + b\gamma^2 + c\gamma + d \tag{25}$$

subject to the following requirements

$$\left.\frac{d^2\xi_\ell}{d\gamma^2}\right|_{\bar{\xi}} = 0 \quad \left.\frac{d\xi_\ell}{d\gamma}\right|_{\bar{\xi}} = 0 \quad \xi_\ell(1) = 1 \quad \xi_\ell(-1) = -1 \tag{26}$$

Here, the subscript ℓ assumes different values as follows: $\ell = 1$ for contour integration; $\ell = 1$ and 2 for area (surface) integration; $\ell = 1$, 2 or 3 for volume integration. Also, $\bar{\xi}$ is the location of the singular point in the local coordinate system. A solution to this problem is given by

$$a = \frac{1}{1+3\bar{\gamma}^2} \quad b = \frac{-3\bar{\gamma}}{1+3\bar{\gamma}^2} \quad c = \frac{3\bar{\gamma}^2}{1+3\bar{\gamma}^2} \quad d = -b \tag{27}$$

where $\bar{\gamma}$ is the value of γ which satisfies $\xi_\ell(\bar{\gamma}) = \bar{\xi}$, calculated by

$$\bar{\gamma} = \sqrt[3]{\bar{\xi}\left(\bar{\xi}^2 - 1\right) + \left|\bar{\xi}^2 - 1\right|} + \sqrt[3]{\bar{\xi}\left(\bar{\xi}^2 - 1\right) - \left|\bar{\xi}^2 - 1\right|} + \bar{\xi} \tag{28}$$

2.3.4 Application of boundary conditions. For a well-posed boundary value problem, every point on the boundary is given either one Dirichlet, one Neumann, or one Robin-type boundary condition. At the same time, the interior heat source function must be known. The known heat source function, {**f**}, can be multiplied by its coefficient matrix, [**e**], to form the known vector {**p**}. The term

[diag **c**] can be absorbed into the diagonal of the matrix [**h**] to form matrix $[\tilde{\mathbf{h}}]$. Equation (20) then results in the following matrix form

$$[\tilde{\mathbf{h}}]\ \{\Theta\} = [\mathbf{g}]\ \{\mathbf{q}\} + \{\mathbf{p}\} \tag{29}$$

The computation of the free term [diag **c**] can be simplified. Rather than computing the geometric internal angle at the ith boundary node, the diagonal of the $[\tilde{\mathbf{h}}]$ matrix can be computed implicitly by considering what would happen if the temperature was constant everywhere and no heat sources were present. In this instance, fluxes would be identically zero. The diagonal, being the only unknown term in this case, can be computed by summing the remaining terms in the BIE so that

$$\tilde{h}_{ii} = -\sum_{j=1}^{N} \tilde{h}_{ij} \tag{30}$$

In the well-posed steady state problems the boundary conditions may be multiplied out and carried to the right-hand-side and added to {**p**} to form a vector of knowns, {**F**}, while the left-hand side remains in the standard form [**A**]{**X**}. Thus, the entire BIE method reduces to a linear algebraic system of the standard form

$$[\mathbf{A}]\{\mathbf{X}\} = \{\mathbf{F}\} \tag{31}$$

The equation set that will result has N unknowns and N equations. It is a well-posed system of linear algebraic equations that can be solved for the unknown vector {**X**} by any appropriate matrix solver.

3 STEADY INVERSE HEAT CONDUCTION PROBLEMS

3.1 Determination of Steady Thermal Boundary Conditions

Inverse determination of unknown steady thermal boundary conditions when temperature and heat flux data are not available on certain boundaries is an ill-posed problem [2–6]. In this case, additional overspecified measurement data involving both temperature and heat flux are required on some other, more accessible boundaries or at a finite number of points within the domain. For example, if at all four vertices of a quadrilateral cell the heat sources are known, at two vertices both $\Theta = \overline{\Theta}$ and $q = \overline{q}$ are known, while at the remaining two vertices neither Θ or q is known, the BIE (Eq. (29)) begins as

$$\begin{bmatrix} \tilde{h}_{11} & \tilde{h}_{12} & \tilde{h}_{13} & \tilde{h}_{14} \\ \tilde{h}_{21} & \tilde{h}_{22} & \tilde{h}_{23} & \tilde{h}_{24} \\ \tilde{h}_{31} & \tilde{h}_{32} & \tilde{h}_{33} & \tilde{h}_{34} \\ \tilde{h}_{41} & \tilde{h}_{42} & \tilde{h}_{43} & \tilde{h}_{44} \end{bmatrix} \begin{Bmatrix} \overline{\Theta}_1 \\ \Theta_2 \\ \overline{\Theta}_3 \\ \Theta_4 \end{Bmatrix} = \begin{bmatrix} g_{11} & g_{12} & g_{13} & g_{14} \\ g_{21} & g_{22} & g_{23} & g_{24} \\ g_{31} & g_{32} & g_{33} & g_{34} \\ g_{41} & g_{42} & g_{43} & g_{44} \end{bmatrix} \begin{Bmatrix} \overline{q}_1 \\ q_2 \\ \overline{q}_3 \\ q_4 \end{Bmatrix} + \begin{Bmatrix} p_1 \\ p_2 \\ p_3 \\ p_4 \end{Bmatrix} \tag{32}$$

In order to solve this set, all of the unknowns will be collected on the right-hand side, while all of the knowns are assembled on the left. A simple algebraic manipulation yields the following set:

$$\begin{bmatrix} \tilde{h}_{12} & -g_{12} & \tilde{h}_{14} & -g_{14} \\ \tilde{h}_{22} & -g_{22} & \tilde{h}_{24} & -g_{24} \\ \tilde{h}_{32} & -g_{32} & \tilde{h}_{34} & -g_{34} \\ \tilde{h}_{42} & -g_{42} & \tilde{h}_{44} & -g_{44} \end{bmatrix} \begin{Bmatrix} \Theta_2 \\ q_2 \\ \Theta_4 \\ q_4 \end{Bmatrix} = \begin{bmatrix} -\tilde{h}_{11} & g_{11} & -\tilde{h}_{13} & g_{13} \\ -\tilde{h}_{21} & g_{21} & -\tilde{h}_{23} & g_{23} \\ -\tilde{h}_{31} & g_{31} & -\tilde{h}_{33} & g_{33} \\ -\tilde{h}_{41} & g_{41} & -\tilde{h}_{43} & g_{43} \end{bmatrix} \begin{Bmatrix} \bar{\Theta}_1 \\ \bar{q}_1 \\ \bar{\Theta}_3 \\ \bar{q}_3 \end{Bmatrix} + \begin{Bmatrix} p_1 \\ p_2 \\ p_3 \\ p_4 \end{Bmatrix} \quad (33)$$

Since the entire right-hand side is known, it may be reformulated as a vector of knowns, $\{\mathbf{F}\}$. The left-hand side remains in the form $[\mathbf{A}]\{\mathbf{X}\}$. Also, additional equations may be added to the equation set if, for example, temperature or heat flux measurements are known at certain locations within the domain. In general, the geometric coefficient matrix $[\mathbf{A}]$ will be non-square and highly ill-conditioned. Most matrix solvers will not work well enough to produce a correct solution.

3.2 Truncated Singular Value Decomposition

There exists a very powerful technique for dealing with sets of equations that are either singular or very close to singular. These techniques, known as Singular Value Decomposition (SVD) methods [39, 29, 46–50], are widely used in solving most linear least squares problems. The goal of the SVD is to choose a solution vector $\{\mathbf{X}\}$ so as to minimize the error

$$E = \|\{\mathbf{F}\} - [\mathbf{A}]\{\mathbf{X}\}\| \quad (34)$$

which is the distance from the point $\{\mathbf{F}\}$ to the point $[\mathbf{A}]\{\mathbf{X}\}$ in the column space. Thus, the solution vector $\{\mathbf{X}\}$ is the projection of $\{\mathbf{F}\}$ onto the subspace which the column vectors of $[\mathbf{A}]$ define. Any M x N matrix $[\mathbf{A}]$ can be written as the product of an M x N column-orthogonal matrix, $[\mathbf{U}]$, an N x N diagonal matrix $[\mathbf{W}]$ with positive singular values, and the transpose of an N x N orthogonal matrix $[\mathbf{V}]$.

$$[\mathbf{A}] = [\mathbf{U}] \begin{bmatrix} w_1 & 0 & 0 \\ 0 & \ddots & 0 \\ 0 & 0 & w_N \end{bmatrix} [\mathbf{V}] \quad (35)$$

The singular values, $w_1,\ldots, w_N$, are the eigenvalues of a matrix $[\mathbf{A}]^T[\mathbf{A}]$. The columns of $[\mathbf{U}]$ corresponding to the nonzero singular values, w_j, make the orthonormal set of basis vectors that span the range of $[\mathbf{A}]$. The columns of $[\mathbf{V}]$ corresponding to the zero singular values, w_j, are an orthonormal basis for the nullspace. If the matrix $[\mathbf{A}]$ is singular, then there is some subspace of $\{\mathbf{X}\}$, called the nullspace, that is mapped to zero, that is, $[\mathbf{A}]\{\mathbf{X}\}=\{\mathbf{0}\}$. Since $[\mathbf{U}]$ and $[\mathbf{V}]$ are each orthogonal in the sense that their columns are orthonormal, the solution vector can be easily found as

$$\{\mathbf{X}\} = [\mathbf{V}][\mathrm{diag}(1/w_j)]\left([\mathbf{U}]^T\{\mathbf{F}\}\right) \quad (36)$$

For a well-conditioned matrix, the singular values w_j will be roughly of the same order of magnitude. The condition number of a matrix is defined as w_{max}/w_{min}. As the condition number increases, the matrix becomes more ill-conditioned. The LU factorization and Gaussian elimination may give a formal solution to an ill-conditioned set of equations, but the solution vector will have highly oscillating components whose algebraic cancellation, when multiplied by the matrix $[\mathbf{A}]$, gives a very poor approximation to the vector $\{\mathbf{F}\}$. Eliminating very

small singular values has the effect of removing those algebraic terms that, because they are dominated by noise and round-off error, produce the oscillating solution vector. In order to determine which singular values are to be eliminated, we must choose a parameter, τ, as a singularity magnitude threshold. Any singular value that satisfies $w_j/w_{max} < \tau$ is zeroed out. In order to zero-out a singular value, one should simply replace the $1/w_j$ by zero. The zeroing of a small singular value corresponds to throwing away one linear combination from the set of equations that is so corrupted by round-off error as to be at best useless. For each particular problem, there is a range of threshold values where the algorithm will produce a correct solution. A choice of the threshold outside of this range will yield another solution vector whose direction is very nearly the nullspace vector. Since the SVD algorithm is capable of solving non-square matrices, the number of unknowns in the equation set need not be the same as the number of equations. Thus, virtually any combination of boundary conditions and internal temperature measurements will yield at least some solution.

3.3 Tikhonov's Regularization

Tikhonov regularization [37, 29] is another type of single-parameter minimization where the solution vector $\{\mathbf{X}\}$ minimizes the weighted sum of the norm of the error vector defined by Tikhonov as

$$E = \|\{\mathbf{F}\} - [\mathbf{A}]\{\mathbf{X}\}\| + \lambda\|\{\mathbf{X}\}\| \tag{37}$$

where λ is the Tikhonov's regularization parameter. We find a minimum error norm by differentiating this equation with respect to each component of the unknown vector, $\{\mathbf{X}\}$, and setting the result equal to zero. After substituting the singular value decomposition and solving for the unknown vector $\{\mathbf{X}\}$, the resulting formulation is as follows

$$\{\mathbf{X}\} = [\mathbf{V}]\left([\mathbf{W}]^T[\mathbf{W}] + \lambda[\mathbf{I}]\right)^{-1}[\mathbf{W}]^T[\mathbf{U}]\{\mathbf{F}\} \tag{38}$$

where $[\mathbf{I}]$ is the identity matrix. Tikhonov regularization is a generalization of least-squares truncation, but instead of simply eliminating terms associated with small singular values, they are weighted by a factor $(1 + \lambda/w^2)$. A low value of λ makes the residual term $[\mathbf{A}]\{\mathbf{X}\} - \{\mathbf{F}\}$ smaller, approaching the least squares solution. Because of the destabilizing effect of the small singular values, the solution for an ill-conditioned matrix oscillates erratically. Larger Tikhonov regularization parameters act as a filter to gradually reduce the effect of the singular values because w_j/w_{max} are less than λ. Thus, the optimal choice of λ provides a balance between the accuracy and the smoothness of the solution. Tikhonov suggested that λ can be found based upon knowledge of the measurement errors [29], that is, λ should be chosen when the least sum of squares lies between

$$\left[N_T - \sqrt{2N_T}\right]\sigma^2 \quad \text{and} \quad \left[N_T + \sqrt{2N_T}\right]\sigma^2 \tag{39}$$

where N_T is the number of temperature measurements and σ^2 is the variance of those measurements.

The level of discretization was found to have no effect on the optimum SVD threshold value, τ_{opt} [9]. The effective range of τ that produced the minimum variance and bias for all levels of discretization was $0.004 \leq \tau \leq 0.08$.

On the other hand, the level of discretization had some influence on Tikhonov's regularization scheme. After the BEM matrices are integrated and the singular value decomposition computed, an iterative quadratic optimization algorithm can be employed [9] in order to determine λ_{opt}. The value of λ can be allowed to vary while the cost function

$$F(\lambda) = w_{var}\,\sigma_{\Theta}^2 + w_{bias}\left(\Theta_{mean} - \Theta_{analytic}\right)^2 \tag{40}$$

is minimized. Here, w_{var} and w_{bias} are user-specified weighting coefficients for the variance, σ_{Θ}^2, and the bias in the non-dimensional temperature. With $w_{var} = w_{bias} = 1$, the optimum Tikhonov's regularization parameter, λ_{opt}, is usually found in 5 to 10 computationally inexpensive iterations [9].

3.4 Results of BEM for Unknown Thermal Boundary Conditions

The accuracy and versatility of the BEM in determining the unknown steady state temperatures and heat fluxes on the boundaries of two- and three-dimensional multiply-connected domains is demonstrated in the following examples. Notice that evaluation of the unknown local values of heat convection coefficient (Eq. (4)) is trivial once the local surface temperature and normal temperature derivative are predicted.

3.4.1 Rectangular plate and finite rod. The accuracy of the BEM as a solution to the two- and three-dimensional steady state ill-posed problem was verified for a rectangular flat plate and a rod having square cross section. The rectangular plate was 6.0 m long by 1.0 m wide. The rod was 6.0 m long by 1.0 m by 1.0 m thick. Thermal conductivity was chosen as $k = 1.0\ W\ m^{-1}\ K^{-1}$ and there were no heat sources, that is, $L = 0$. The long sides of the plate and rod were specified to be adiabatic ($-k\bar{Q} = 0\ W\ m^{-2}$) while at one end, the boundary conditions were overspecified with a temperature of $\bar{T} = 300.0$ K and a heat flux of $-k\bar{Q} = -50.0\ W\ m^{-2}$. The boundary at the opposite end was considered to be inaccessible and, as such, both temperature and heat flux were unknown there. The rectangular plate was discretized with 14 linear elements (6 per each of the two sides and 1 on each end). The rod surface was discretized with 26 square flat panels (6 per each of the four sides and 1 on each end). Both two- and three-dimensional BEM numerical formulations of the UIHCP were highly successful in computing a linear temperature field within the rod that was accurate to almost the floating point precision of the computer. The predicted temperatures and heat fluxes at the end of the plate and the rod (where no boundary conditions were given) were $\bar{T} = 0.00001$ K and $-k\bar{Q} = -49.99997\ W\ m^{-2}$, respectively, compared to the analytic solutions of $\bar{T} = 0$ K and $-k\bar{Q} = -50.0\ W\ m^{-2}$.

3.4.2 Annular disk. The behavior of the BEM algorithm for various combinations of boundary conditions can be demonstrated for steady-state heat conduction in a two-dimensional, annular, concentric circular disk with no heat

sources [2, 3]. In the well-posed (analysis or direct or forward) case of no heat sources and constant temperatures imposed on the entire outer and inner circular boundaries, the analytic solution for the resulting Laplace's equation for the Kirchhoff's non-dimensional temperature is easily found as

$$\Theta(\rho) = c_1 + c_2 \ln \rho \tag{41}$$

where $\rho = r/\ell$. In our test case, the non-dimensionalized outer radius of the annular disk was $\rho_{outer} = 1.2$ and the centrally located circular hole had a non-dimensional radius of $\rho_{inner} = 0.5$. The analytic solution for a well-posed Dirichlet analysis problem was obtained by applying $\bar{\Theta}_{outer} = 1.0$ on the outer circular boundary and $\bar{\Theta}_{inner} = 0.5$ on the inner circular boundary of the annular domain. For these parameters the analytic values of the integration constants were $c_1 = 0.8959$ and $c_2 = 0.5712$. The corresponding analytic values of the radial non-dimensional heat fluxes are $\bar{q}_{outer} = 0.4759$ and $\bar{q}_{inner} = 1.1422$. The accuracy of our BEM algorithm in its analysis mode was verified on the same test case. The geometry was discretized with 36 equal-length linear isoparametric boundary elements on each outer and inner circular boundary. The BEM program predicted the non-dimensional temperature in the entire annular domain which averaged only a 0.1% negative bias error and 0.0001 standard deviation versus the analytic solution.

In order to study the feasibility and accuracy of the BEM solution to the steady inverse heat conduction problem (SIHCP), four variations of the given problem were performed and the results obtained were compared to the analytic solution. In all the test cases, a constant temperature was specified on the entire outer circular boundary. At the same time, both temperature and the heat flux were treated as unknown on the entire inner circular boundary. The test cases are summarized in Table 1.

Test 1. The entire outer boundary was overspecified with constant flux boundary conditions. The BEM computed the non-dimensional temperature field within the annular domain in addition to the unknown non-dimensional temperatures and heat fluxes on the inner boundary. The computed isotherms (Fig. 1a) for the annular solid disk demonstrate an almost perfectly symmetric result with an average error of 0.5% in non-dimensional temperature and a somewhat oscillating error in heat flux averaging about −1.5%.

Test 2. The heat flux boundary conditions were overspecified on the outer circular boundaries of the first and third quadrants only. The computed non-dimensional temperature distribution on the inner boundary was somewhat oscillatory (Fig. 1b), but averaged only a 0.75% error. The predicted heat flux on the inner boundary averaged an error of about −2.0%.

Test 3. The heat flux boundary conditions were overspecified only on the upper half of the outer circular boundary. The computed non-dimensional temperature field is asymmetric about the horizontal centerline (Fig. 1c), but shows a nearly perfect symmetry about the vertical centerline. The error of the predicted non-dimensional temperature on the inner boundary peaks to 24%. The errors in computed fluxes peak to about 40% at the point farthest from the overspecified data.

Test 4. The heat flux boundary conditions were overspecified on the outer boundary of the first quadrant only. The error in the predicted non-dimensional temperature field worsens as the distance from the overspecified data increases (Fig. 1d) and peaks to 60% at the point farthest from the overspecified data. Notice

also that the predicted non-dimensional temperature field is symmetric about the line inclined 45 degrees and passing through the center of the circle.

Table 1 Important parameters for the annular disk SIHCP cases

Test case	Number of known values (Θ and q)	Number of unknown values (Θ and q)	Number of algebraic equations
1	72	72	72
2	54	90	72
3	54	90	72
4	45	99	72

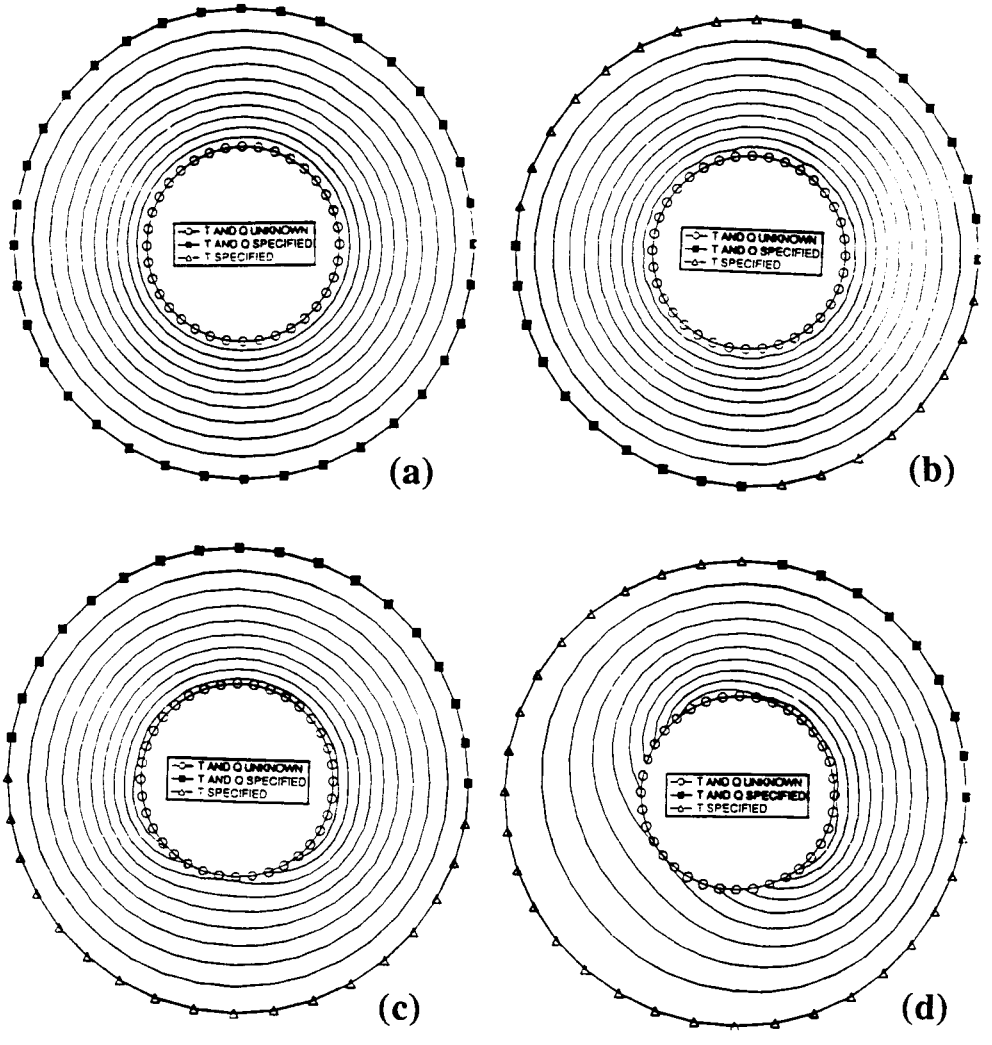

Figure 1 Isotherms predicted with the inverse BEM in an annular circular disk with specified constant temperature only (triangles) and both temperature and heat flux (full squares). Nothing was specified on the entire inner circular boundary (circles). The over-specified boundary conditions were on (a) the entire outer boundary, (b) the first and the third quadrant of the outer boundary, (c) the upper half of the outer boundary, and (d) the first quadrant of the outer boundary.

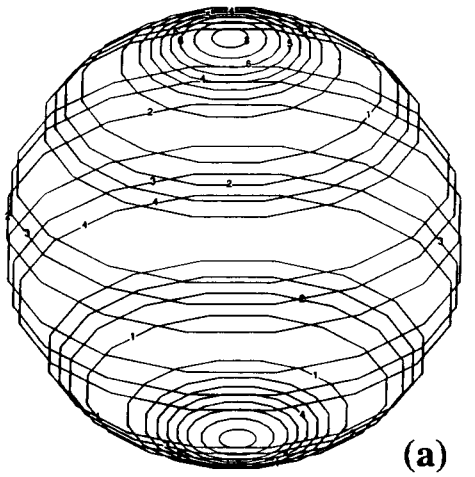

(a)

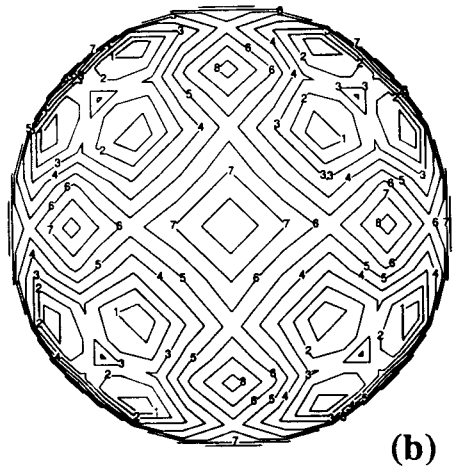

(b)

Level	T
8	58.3164
7	56.7609
6	55.2053
5	53.6498
4	52.0942
3	50.5387
2	48.9831
1	47.4276

Level	T
8	52.154
7	51.607
6	51.06
5	50.513
4	49.966
3	49.419
2	48.872
1	48.325

Level	Flux
8	-172.063
7	-172.626
6	-173.19
5	-173.753
4	-174.317
3	-174.88
2	-175.444
1	-176.007

Level	Flux
8	-128.678
7	-140.256
6	-151.833
5	-163.411
4	-174.989
3	-186.567
2	-198.144
1	-209.722

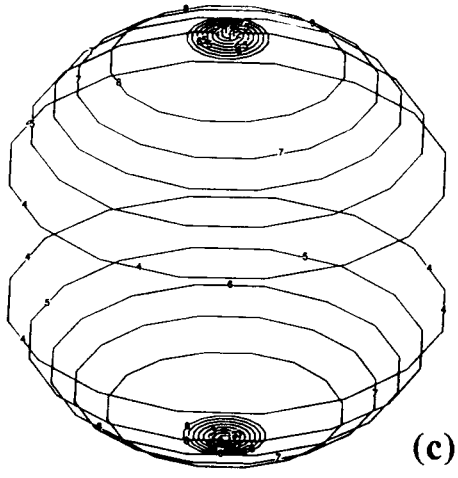

(c)

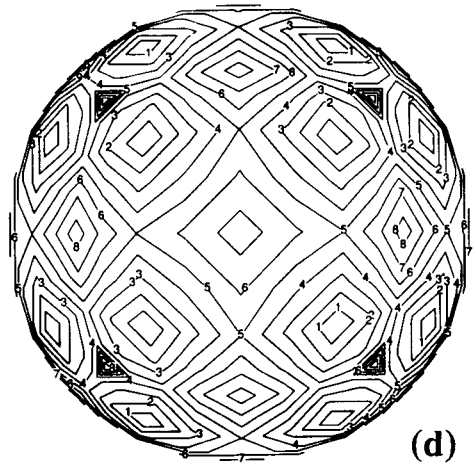

(d)

Figure 2 Thermal boundary conditions predicted on the surface of a spherical cavity when temperature and heat flux were specified on the entire outer spherical boundary and nothing was specified on the concentric spherical cavity. Isotherms predicted with a meridional surface grid (a) and a cube-to-a-sphere expanded grid (b) and fluxes predicted with a meridional surface grid (c) and a cube-to-a-sphere expanded grid (d) .

3.4.3 Sphere within a sphere. The BEM solution to the SIHCP was also exercised on a simple three-dimensional geometry consisting of a sphere of radius r = 1.2 m with a concentric spherical cavity of radius r = 0.5 m. With k = 1.0 W $m^{-1} K^{-1}$, $\bar{T}_{outer}$ = 100.0 K, $\bar{T}_{inner}$ = 50.0 K, and L = 0, the analytic solution is $T(r) = c_1 + c_2/r$ where c_1 = 135.72 K and c_2 = −42.86 K m. We then used isoparametric bilinear quadrilateral panels to discretize the spherical boundaries [3]. The surface grids were used at various levels of refinements, including 8, 10, 12 and 16 boundary elements (panels) both longitudinally and latitudinally on the outer and inner spherical boundary. The analysis version of the BEM solved for the fluxes, Q, on the outer and inner spherical boundaries. The numerical result contained a biased error of 2% that was concentrated at the poles for all levels of grid refinement.

The SIHCP problem was then formulated by overspecifying the outer spherical boundary (applying both temperature and flux from the analytic solution), while not providing any thermal boundary conditions on the inner (cavity) spherical boundary. The BEM-predicted temperatures (Fig. 2a) and heat fluxes (Fig. 2b) on the surface of the spherical cavity, with the discretization of 16x16 quadrilateral bilinear panels, illustrate biased errors up to 16% in temperature and 3% in heat flux at the poles since the analytic solution is $-k\bar{Q}_{inner} = -171.44$ W m^{-2}. The error of the SIHCP was the greatest at the poles because the boundary grid of bilinear quadrilateral cells deforms to nearly triangular cell shapes adjacent to the poles. These boundary cells behave very poorly because the approximating polynomials are not well-behaved in these regions. In addition, it is difficult to carry out the integration over these polar surface integrals properly due to the nature of the singular fundamental solution. Moreover, when observation nodes are very close to the boundary element of integration, the accuracy of the numerical quadrature integration scheme deteriorates.

We then repeated the SIHCP with a different surface grid pattern. First, a cube was discretized with 16 bilinear quadrilateral boundary elements on each of its six sides. A cubical hole centered within the first cube was discretized with the same type of grid. The surface grids of both cubes were then expanded radially to a sphere-within-a-sphere configuration. The same SIHCP was then solved using our BEM algorithm with Tikhonov's regularization parameter $\lambda = 1.0 \times 10^{-12}$. This provided a slightly better result than the SVD matrix solver for the predicted temperatures on the surface of the spherical cavity. These results show a maximum unbiased error in temperature of about 4% (Fig. 2c). The errors in fluxes were quite large (Fig. 2d), maximizing to 22% at what would be the corners of the original cubical cavity. The results did not improve or worsen for other levels of discretization. During the expansion of the cube-within-a-cube grid into a sphere-within-a-sphere grid the quadrilateral cells are stretched adjacent to what used to be the corner nodes of the cubes. The BEM is sensitive to geometric distortions in isoparametric elements. The Jacobian of the nearly triangular boundary elements was found to be almost zero at the vertices of these elements. Other isoparametric boundary elements such as triangles and higher-order quadrilaterals should be attempted to remedy this problem.

3.4.4 Treatment of geometries with corners. The accuracy of the ill-posed BEM formulation was shown (Figs. 1c−1d) to deteriorate as the amount of overspecified data decreases and when the distance from the overspecified data increases. We have also noticed that the accuracy of this approach deteriorates when only Dirichlet boundary conditions are specified across a sharp corner.

In the implementation of the direct BEM for the solution of the heat conduction equation, the heat flux at a corner is double-valued due to the non-

uniqueness of the outward normal. This fact poses a numerical problem at nodes located at these corners. There are three variables at such nodes, the temperature and two normal temperature derivatives, and only one boundary integral equation is available. Dirichlet boundary conditions provide only one of the three unknowns for each corner node. When the corner node is on an inaccessible boundary, nothing is provided there. In these cases, one additional equation must be provided. This condition can be satisfied using the discontinuous element formulation [43, 44] or by developing an expression that relates the normal and tangential temperature derivatives to a unique temperature gradient [51]. Although these approaches work well in the analysis or well-posed problems, difficulties arise when the ill-posed or inverse problems are encountered. So far, we have found no universally adequate formulation for the accurate treatment of corners for the ill-posed problem.

As an example of the properly treated corners, a well-posed problem was constructed for the geometry of a cross-shaped hole within a square plate with f = 0. The outer boundary of the square plate was specified with $\bar{\Theta}_{outer} = 1.0$ and the inner, cross-shaped boundary was specified with $\bar{\Theta}_{inner} = 0$. The outer and the inner boundary were discretized with 60 linear isoparametric equal-length boundary elements, respectively. The results of the BEM analysis of this well-posed Dirichlet problem (without f = 0) are shown as a plot of computed isotherms (Fig. 3a).

Next, the fluxes on the outer square boundary that were computed by the analysis BEM solution were applied in addition to $\bar{\Theta}_{outer} = 1.0$ as overspecified boundary conditions. This time, nothing was specified on the boundary of the cross-shaped hole. The BEM developed a solution to this SIHCP. The predicted non-dimensional temperature field around the cross-shaped hole appear to have been predicted quite accurately (Fig. 3b).

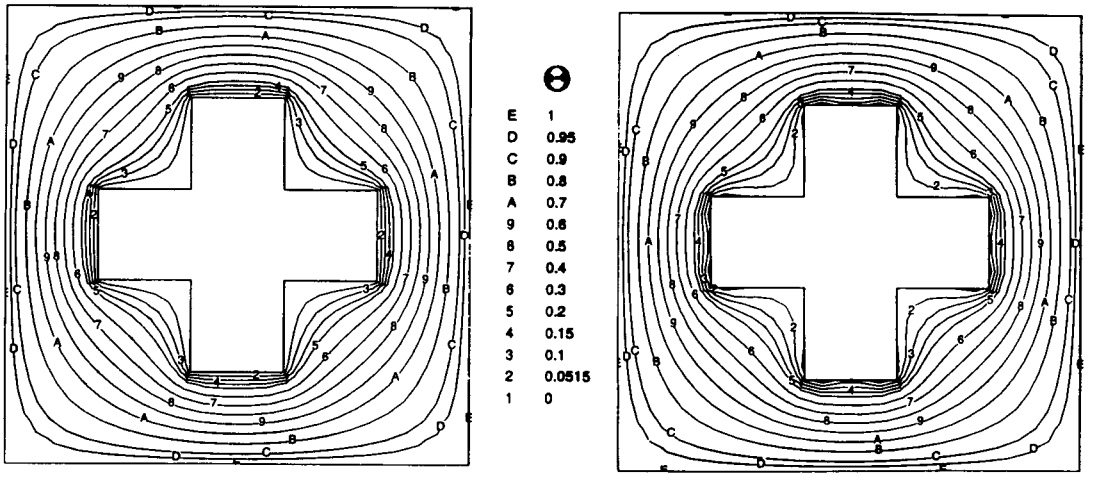

Figure 3 Isotherms predicted using BEM in a square plate with a cross-shaped central hole. Well-posed problem (temperatures given on both entire inner and outer boundaries) results (a) and inverse problem (temperatures and heat fluxes given on the outside boundary and nothing provided on the boundaries of the cross-shaped hole) results (b).

3.4.5 Two-dimensional section of a cooled rocket chamber wall. The ill-posed BEM formulation was attempted on a realistic engineering design problem with temperature-dependent material properties. High pressure, reusable rocket thrust chambers encounter progressive thinning of the coolant passage wall after repetitive engine operation [52]. This deformation is caused by high thermal plastic deformations and recrystalization that eventually cause cracks to form in the coolant passage wall. An engineer who wishes to reduce or eliminate the plastic strain by reshaping the coolant flow passage may obtain experimental data such as nozzle shroud temperatures and heat fluxes. Unfortunately, the engineer cannot obtain data within a coolant flow passage due to the extremely low temperature of the liquid hydrogen coolant and the small dimensions of the passages.

The hot gas wall (left boundary in Fig. 4a) was specified with $-k\bar{Q}_{hot} = -57.24 \times 10^6$ W m^{-2}. The outer shroud (right boundary in Fig. 4a) heat flux was assumed to be negligible ($\bar{Q}_{outer} = 0$). The shroud was overspecified with a temperature of $\bar{T}_{outer} = 288.0$ K taken from experimental measurements [52] and there were no heat sources (f = 0). The circumferentially-periodic meridional boundaries of the nozzle wall section (top and bottom boundaries in Fig. 4a) were also specified to be adiabatic $(\partial\bar{T}/\partial\theta) = 0$.

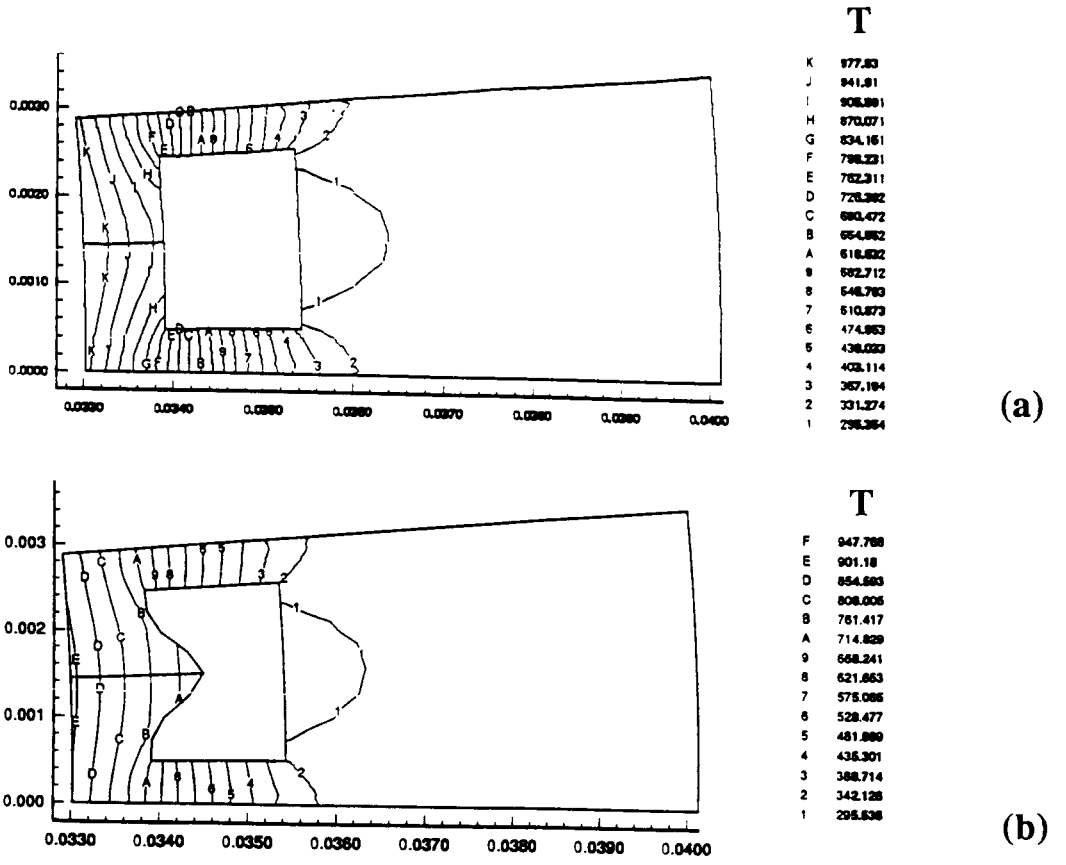

Figure 4 Isotherms predicted inside a circumferentially-periodic segment of a rocket nozzle wall with a cooling channel when nothing was known on the boundaries of the cooling channel. Results of the inverse boundary condition code for a rectangular channel (a) and for a channel with a rounded fin (b).